A compact *in-situ* polarized ^{3}He system for neutron scattering

Jian Tang,[1,2,3,4,*] Bin Wang,[1,2,4,5,*] Chuyi Huang,[6] Han Gao,[1,2,4] Qingbo Zheng,[1,2,3,4] Renhong Liu,[1,2,4] Fan Ye,[1,2,4] Zecong Qin,[1,2,4] Tianhao Wang,[1,2,3,4] Ahmed Salman,[1,2,4] Yuchen Dong,[1,2,3,4] Long Tian,[1,2,4] Changdong Deng,[1,2] Jun Li,[1,2] Lei Liu,[1,2] Xin Qi,[1,2,4] Junpei Zhang,[1,2,3,4,†] and Xin Tong[1,2,3,4,‡]

[1] *Institute of High Energy Physics, Chinese Academy of Science(CAS), Beijing 100049, China*
[2] *Spallation Neutron Source Science Center, Dongguan 523803, China*
[3] *University of Chinese Academy of Sciences, Beijing 100049, China*
[4] *Guangdong Provincial Key Laboratory of Extreme Conditions, Dongguan 523803, China*
[5] *Center for Neutron Science and Technology, Guangdong Provincial Key Laboratory of Magnetoelectric Physics and Devices, School of Physics, Sun Yat-Sen University, Guangzhou 510275, China*
[6] *Jülich Centre for Neutron Science at MLZ, Lichtenbergstr. 1, 85747 Garching Germany;*

(Dated: January 12, 2025)

The performance of a new compact (55 cm × 56 cm × 48 cm) *in-situ* spin-exchange optical pumping (SEOP) ^{3}He-neutron spin filter (NSF) system developed at the China Spallation Neutron Source (CSNS) is presented. The enclosed NSF cell, filled with 2.53 bar ^{3}He, was born with a ^{3}He polarization of around 60%. After subsequent improvements to the magnetic field and heating system, this *in-situ* system is able to achieve 75.66%±0.09% ^{3}He polarization, resulting in a 96.30% neutron polarization at 2 Å. This highly compact *in-situ* system is equipped with self-supportive features, pre-pumping capabilities, polarization maintenance, and low-noise Nuclear Magnetic Resonance (NMR) system. These advantages significantly reduce the preparation time and simplify the processes in polarized neutron experiments, allowing it to be adopted on various neutron beamlines in China, especially those with limited sample space. These characteristics establish it as a quasi-standardized system, playing a vital role in polarized neutron experiments including polarized neutron imaging, neutron reflection, the performance calibration of polarized neutron instruments, Neutron Optics Parity and Time Reversal EXperiment (NOPTREX).

I. INTRODUCTION

Polarized neutron technology has important applications in neutron scattering experiments, especially in advanced material research [1][2][3][4]. Generally, three technologies are employed to achieve polarized neutrons: Heusler crystals [5], polarizing supermirror [6], and polarized ^{3}He [7]. Compared with Heusler crystals and polarizing supermirror, polarized ^{3}He has the advantages of large scattering angle, low background, wide energy spectrum, uniform polarization and neutron flipping ability, which make polarized ^{3}He widely used over the past few decades [7][8].

Polarized ^{3}He can be mainly produced through either metastability-exchange optical pumping (MEOP) [9][10] or spin-exchange optical pumping (SEOP) [11][12]. The SEOP method offers a compact size and allows for easy installation into instruments, and the initial investment cost is almost one tenth of that of a MEOP system [13]. Furthermore, the *in-situ* SEOP method can continuously polarize the neutron spin filter (NSF) and thus does not need decay calibration and daily shift. Our previous work involved the development of *off-situ* ^{3}He NSF [14] and the first generation *in-situ* ^{3}He system (*in situ* 1) at CSNS [15], which supplied NSFs to some neutron beamlines. However, they suffered from slow decay of ^{3}He polarization [16] or large sizes, respectively, which limited their utility on the spectrometers with restricted space. To address the decay and large size limitations, we have developed a compact *in-situ* NSF system. The new system has been significantly reduced in volume by nearly 1/2, reducing the load on beamline support, and fitting into tight spaces for sample analysis in neutron experiments. Moreover, the ^{3}He polarization of the new system has reached 75.66%±0.09% as measured by neutrons. Therefore, it provides a powerful tool and great convenience for neutron scattering experiments. The development and commission of the compact *in-situ* ^{3}He system are described thoroughly in this paper.

II. THE COMPACT *IN-SITU* SYSTEM

The primary challenge in constructing a more compact *in-situ* NSF system is to minimize its length along the neutron pathway. Therefore, the guide field, magnet, and optical parts settled on the beam path need to be optimized to release enough space and meet the space requirement of the spectrometers. Finally, the new *in-situ* system is designed to be 55 cm in width (along the neutron beam path), 56 cm in length, and 48 cm in height, with an overall weight of less than 50 kg. The system is self-supported and equipped with a height adjustable function. The self-supporting cart is designed with a table size of 70 cm × 63 cm and a weight of less than 200 kg, which can be adjusted between 143 cm

* These authors contributed equally to this work.
† Corresponding author. Email:zhangjunpei@ihep.ac.cn
‡ Corresponding author. Email:tongxin@ihep.ac.cn

and 230 cm in height. This structure helps the system to accommodate the neutron beam heights of different spectrometers. Its mechanical design is schematically shown in Fig. 1. In Fig. 1 (a), the *in-situ* NSF system employs four fans to facilitate heat exchange, ensuring stable internal temperatures. Inside the box, the laser, heating, magnetic field, NSF and optical systems are integrated. In Fig. 1 (b), the supporting equipment is stored within the frame, including Function Generator (Func Gen), Data Acquisition (DAQ), System Control (Sys-Control), Magnet Driver (Mag-Driver), Uninterrupted Power Supply (UPS), chiller, computer, and other slave equipment. The parameters of the *in-situ* system are detailed as follows:

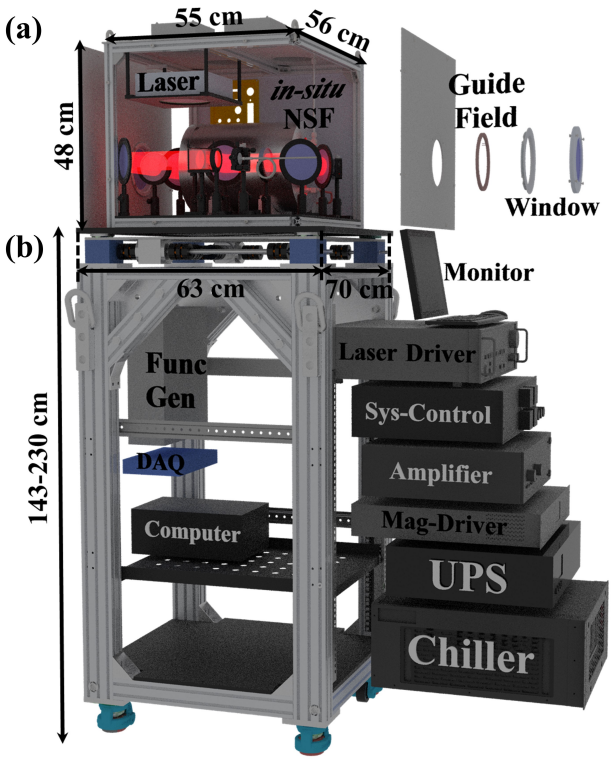

FIG. 1: Schematic of the compact *in situ* system. The optical setup can be found in [15]. (a) NSF part. (b) supporting part. Here, Func Gen: Function Generator, DAQ: Data Acquisition, Sys-Control: System Control, Mag-Driver: Magnet Driver, UPS: Uninterrupted Power Supply.

Magnetic system: The magnetic field system is crucial for the polarization of ^{3}He [11]. Due to size limitations, the priority is to squeeze the size of the magnet system for a compact *in-situ* NSF system. A solenoid was designed to comprise 266 turns, with a diameter of 25.5 cm and a length of 33.2 cm. It was compensated by two pairs of coils, consisting of 5 turns and 18 turns, respectively. These coils are wound with ϕ =1 mm copper wire, and the driving currents of them can be adjusted individually to compensate for magnetic field uniformity. Additionally, a 2 mm thick μ metal layer was hired to shield the stray field and provide a robust magnetic field for the SEOP process. The simulation result of magnetic field analyzed by the finite element analysis software COMSOL [17] is shown in Fig. 2. The magnetic field distribution in the solenoid and the NSF are shown (see Fig. 2 (a) and (b)), and the volume averaged transverse gradient of NSF is 1.74×10^{-4} /cm (see Fig. 2 (c)).

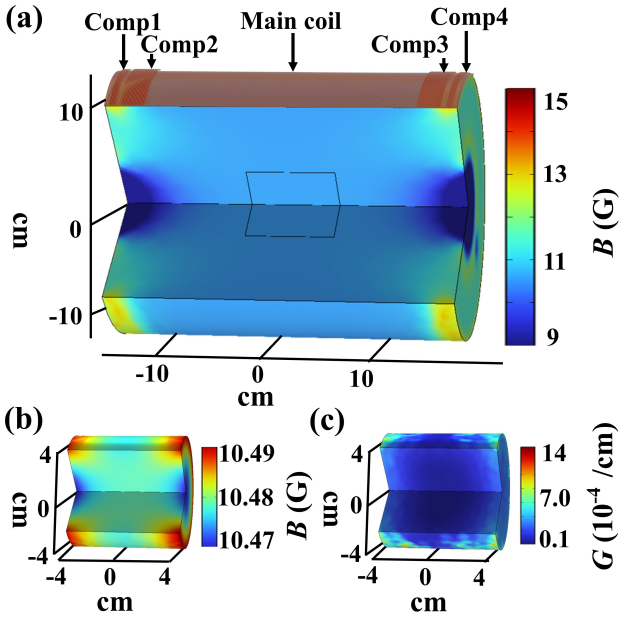

FIG. 2: (a) Simulated magnetic field in the solenoid. (b) Simulated magnetic field in the NSF region with the geomagnetic field environment. (c) Simulated magnetic field standardized transverse gradient of the NSF.

During the optimization of the magnetic field, a correlation between the magnetic field gradient relaxation time $T_1^{\rm fg}$ ($\propto\frac{1}{|\vec{\nabla}B_x|^2+|\vec{\nabla}B_y|^2}$, $\frac{1}{T_1}=\frac{1}{T_1^{\rm fg}}+\frac{1}{T_{\rm wall}}+\frac{1}{T_{\rm dipole}}$) and the relaxation time T_2 ($\propto\frac{1}{|\vec{\nabla}B_z|^2}$) of the Free Induction Decay (FID) signal [18][19] was derived, which is shown Eq. (1). Here, the deduction of the correlation is mainly based on current, where the positive constant b depends only on the shape, pressure, and temperature of the NSF [18]. $\vec{\nabla}B_x$, $\vec{\nabla}B_y$, and $\vec{\nabla}B_z$ are the magnetic field gradients at the location of the NSF [18][19], in addition, $\xi(a,x,y,z)$ is a positive constant function that depends only on the radius (a) of the compensation coils and the position (x,y,z) of the FID coil, the detailed derivation can be found in [20]. Therefore, the magnetic field can be addressed through fine-tuned current by monitoring the transverse re-

laxation time T_2 signals of two FID coils. After improving the relaxation time T_2 from 12 ms to a maximum of 18 ms, combine the action of other subsystems, the ^{3}He polarization has increased from 60.09% to 68.70% by the Electron Paramagnetic Resonance (EPR) measurement [16][21].

$$\frac{T_2}{T_1^{\mathrm{fg}}} = b \times \frac{|\vec{\nabla}B_x|^2 + |\vec{\nabla}B_y|^2}{|\vec{\nabla}B_z|^2} = b \times \xi(a,x,y,z) \qquad (1)$$

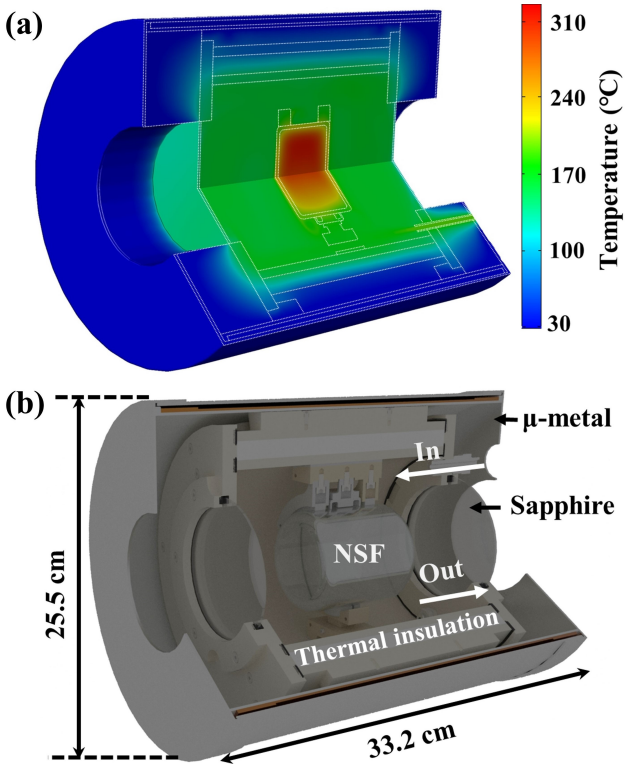

FIG. 3: (a) Simulated temperature distribution inside the oven. (b) Geometry inside the oven.

Heating and laser system: In typical SEOP process [11], the ^{3}He NSF cell needs to be heated to approximately 200 °C to generate sufficient alkali metal vapor. Based on previous work, a temperature distribution will be generated in the NSF [22]. To improve the performance of the heating system, the oven was optimally designed through thermal simulation by the finite element analysis software ANSYS [23], which provides a uniform heating circumstance for the NSF, as shown in Fig. 3 (a). Compared to *in situ* 1 system [15], the volume of the oven for the new compact system has been reduced by 70%, as shown in Fig. 3 (b). The control process of the heating system is shown in Fig. 4 (a). A fuzzy Proportional Integral Derivative (PID) algorithm was adopted to control the oven temperature. After carefully adjusting the parameters of the fuzzy PID algorithm, the precision of temperature control of the heating system has been significantly improved. Additionally, the silicon dioxide thermal insulation layer (≈ 1 cm thick), with a thermal conductivity of 0.017 W/(m · K), effectively reduces the pressure on the heat dissipation and μ metal shielding. The oven can now be heated up to 195 °C within 0.5 hours (h) and maintained a temperature accuracy within ±0.15 °C. The actual temperature data of the NSF surface during the heating is shown in Fig. 4 (b).

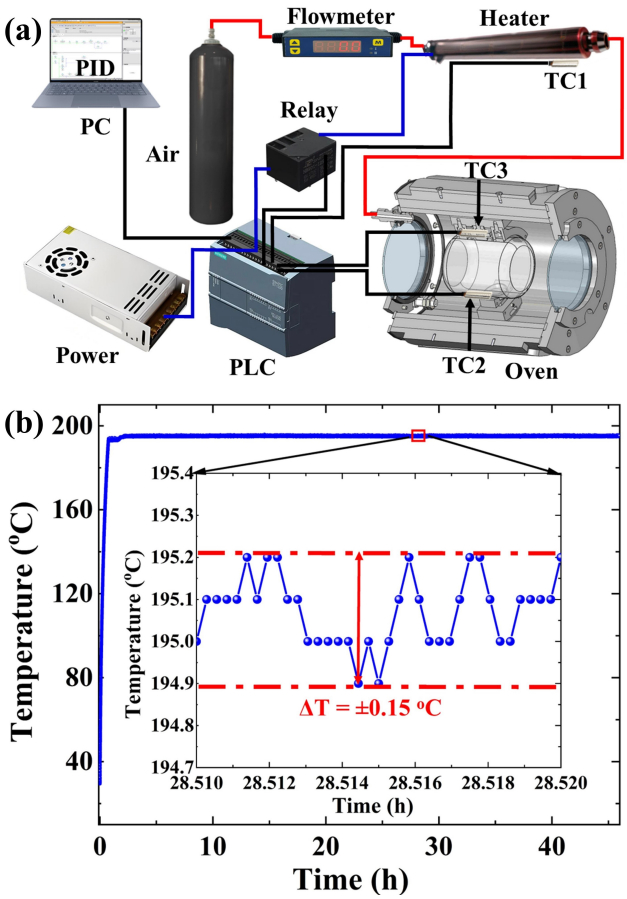

FIG. 4: (a) The control process of the heating system. (b) The actual temperature measured on the NSF surface.

The optical setup of this compact system is similar to the previous system [15], with the lens, polarizing beam splitter, high laser reflecting and neutron transparent mirror, and quarter wave plate positioned in the pumping path. A narrow line width (0.2 nm) high power pumping laser, delivering a total power of 160 W, is employed to provide circularly polarized light for polarizing the alkali atom. A pair of anti-reflective coated sapphire windows is used to enhance the penetration of the pump laser, which can also preserve the heat and neutron

transmission. Additionally, a corresponding interlock system is installed to ensure the safe operating of the laser and heating system.

Neutron spin filter (NSF): The installed cylindrical ^{3}He NSF, made of GE180, was produced in the filling station at CSNS [24]. It has dimensions of 8.0 cm in outer diameter, 8.0 cm in outer length, and a 0.4 cm wall thickness, resulting in an actual neutron path length of 7.2 cm for ^{3}He. The ^{3}He pressure was calibrated as 2.53 bar at 25 °C by neutrons at BL-20 CSNS using the same method as previous work [14].

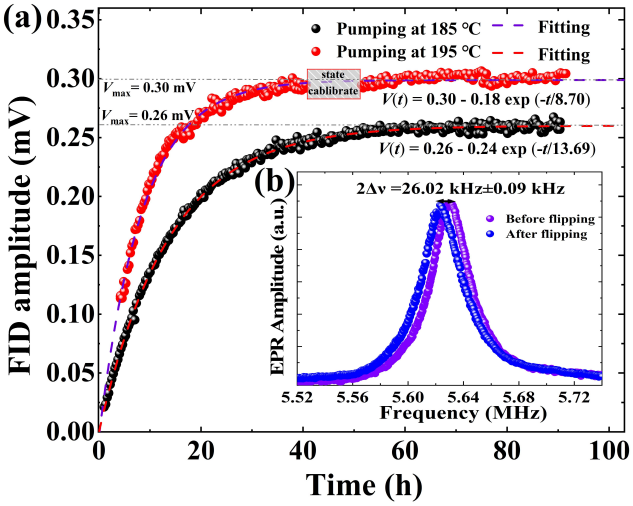

FIG. 5: (a) The FID signal amplitude during the pumping process under 185 °C and 195 °C. (b) Schematic of the EPR signal, with a frequency shift of $2\Delta\upsilon$ = 26.02 kHz±0.09 kHz.

Nuclear magnetic resonance (NMR) system: The NMR system incorporates Free Induction Decay (FID) technology [16], Electron Paramagnetic Resonance (EPR) technology [16][21], and Adiabatic Fast Passage (AFP) technology [25][26]. FID technology primarily monitors the state of polarized ^{3}He. After carefully insulating the ground and filtering the power supply, the signal-to-noise ratio (SNR) of the FID signal reaches 25 when saturated. The pumping data indicated that the spin-up time constants were 13.69 hours at 185 °C and 8.70 hours at 195 °C, there was an obvious increase for FID signal after the temperature increase, as shown in Fig. 5 (a). Meanwhile, the combination of EPR with AFP technologies enables the precise measurement of absolute ^{3}He polarization. The AFP flipping loss was measured at 0.3% per flip during the experiment. Additionally, the EPR frequency shift of 26.02 kHz±0.09 kHz was measured at 195 °C, as shown in Fig. 5 (b), which indicates a ^{3}He polarization of 77.48%±0.25%.

III. COMMISSIONING ON THE NEUTRON BEAMLINE

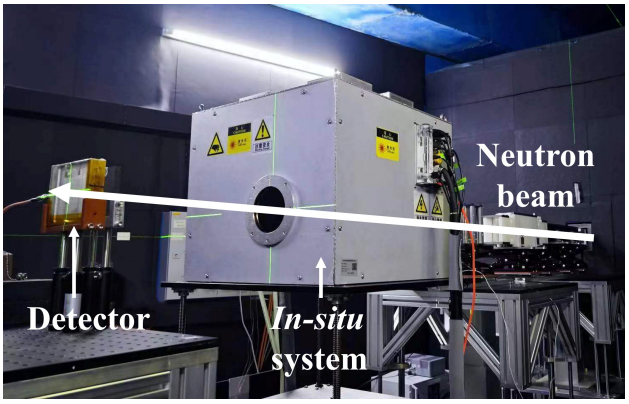

FIG. 6: Installation of the *in-situ* system on BL-20.

The *in-situ* NSF system has been calibrated on BL-20 with neutrons of 1.2-5.2 Å at the CSNS, as shown in Fig. 6. The polarization of ^{3}He, denoted as $P_{^3\mathrm{He}}$, can be derived from the neutron transmission T_n through the ^{3}He NSF as [24]:

$$T_\mathrm{n} = T_\mathrm{e}\exp(-n\sigma l)\cosh(n\sigma l P_{^3\mathrm{He}}) \quad (2)$$

T_0 is the neutron transmission for the fully depolarized ^{3}He. According to Eq. (2), ^{3}He polarization can be fitted as 75.66%±0.09%, as shown in Fig. 7.

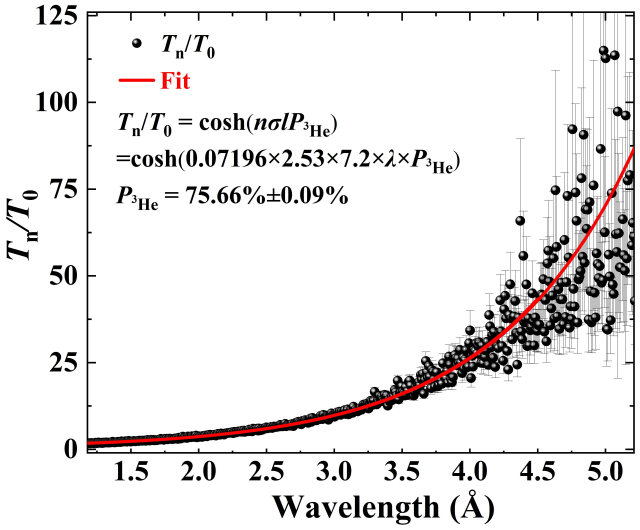

FIG. 7: The fitting of ^{3}He polarization at 1.2-5.2 Å wavelength.

For a ^{3}He NSF, its Figure of Merit (FOM) is defined as $Q = P_\mathrm{n}^2 T_\mathrm{n}$, where $P_\mathrm{n} = \tanh(n\sigma l P_{^3\mathrm{He}})$ is neutron polarization and T_n is neutron transmission [16]. As shown in Fig. 8, the neutron polarization achieves 96.30% at 2.0 Å, while Q attains a peak value of 0.226 at 1.50 Å.

TABLE I: The performance parameters of some *in-situ* polarized ^{3}He systems in the world.

Insitu system	China, CSNS (this system)	China, CSNS [15]	UK, ISIS [27]	Germany, MLZ [28]	USA, SNS [29]	USA, HFIR [12]	Japan, J-PARC [30][31]
$P_{^3He}$	75.56%	74.40%	63.00%	78.50%	84.00%	55.00%	73.00%
P_n	83.03%	64.54%	62.40%	99.38%	83.42%	81.46%	78.79%
p (bar)	2.53	1.58	1.69	3.00	2.30	3.00	3.76
V (cm^3)	55×56×48	70×70×60	85×65×45	62×20×40	69×59×54	30×66×44.5	60×60×30
d (cm)	8.0	7.2	11.0	5.0	7.0	5.8	3.4
l (cm)	8.0	8.7	8.8	15.0	8.0	8.8	5.3
L (cm)	55	70	85	62	69	30	60

$P_{^3He}$: ^{3}He polarization, P_n: neutron polarization at 1.2 Å, p: NSF pressure, V: *in-situ* system dimension, d: NSF diameter, l: NSF length, L: neutron pathway length of *in-situ* system.

The performance parameters of *in-situ* polarized ^{3}He systems used by different neutron sources are shown in Table 1. It shows that the performance of the this *in-situ* system has reached the international advanced level.

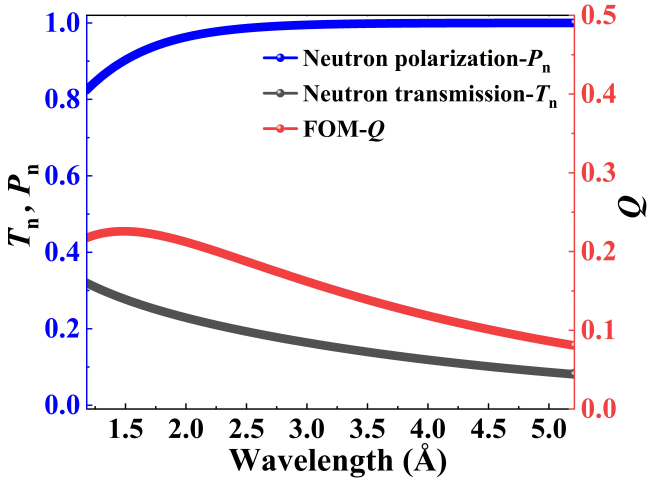

FIG. 8: Performance of the *in-situ* NSF system as a function of the neutron wavelength. T_e= 0.85 is assumed for all calculations in this paper.

IV. CONCLUSIONS

In conclusion, we have successfully developed a new compact *in-situ* NSF system. The new system meets the requirements of half of existing spectrometers space configurations and the ongoing construction of new neutron beamlines at CSNS.

In addition, systematic modifications and optimizations have been made on the magnetic field, heat transfer, hosting system, and noise filtering to achieve the best ^{3}He polarization of 75.66%±0.09%, as measured by the neutrons for a 2.53 bar ^{3}He NSF, enabling a 96.30% neutron polarization at 2 Å. The characteristics of the *in-situ* system make it an ideal polarizer and analyzer for polarized neutron experiments. Currently, this *in-situ* system has been employed in the neutron experiments of the multipurpose reflectometer at CSNS (MR, CSNS [32]), the test beamline (BL-20, CSNS), the back-streaming neutron line (Back-n, CSNS [33]), and the cold neutron imaging beamline at the China Advanced Research Reactor (CNGC, CARR). Moving forward, we remain committed to enhancing the performance of the *in-situ* system to improve polarized neutron applications.

This work was supported by the National Science Fund for Distinguished Young Scholars (Grant No. 12425512), National Key Research and Development Program of China (Grant No. 2020YFA0406000), National Natural Science Foundation of China (Grant No. 11875265), Scientific Instrument Developing Project of the Chinese Academy of Sciences (Grant No. ZDKYYQ20190004), Guangdong Basic and Applied Basic Research Foundation (Grant No. 2019B1515120079), and Dongguan Introduction Program of Leading Innovative and Entrepreneurial Talents (Grant No. 20191122), Guangdong Provincial Key Laboratory of Extreme Conditions, Dongguan Key Laboratory. We give special thanks to our glassblower Junsong Xie, who has been supportive in this project since the beginning. We are grateful to Dr. Songlin Wang for his guidance during the neutron tests on BL-20 at the CSNS.

V. REFERENCES

[1] Hang X D, Matsuda M, Held J T, Mkhoyan K A and Wang J P 2020 Phys. Rev. B 102 104402
[2] Krycka K, Borchers J, Ijiri Y, Booth R and Majetich S 2012 J. Appl. Cryst. 45 554-565
[3] Niketic N, van den Brandt B, Wenckebach W Th, Kohlbrecher J and Hautle P 2015 J. Appl. Cryst. 48 1514-

1521.
[4] Petsch A N, Zhu M, Enderle M, Mao Z Q, Maeno Y, Mazin I I and Hayden S M 2020 Phys. Rev. Lett. 125 217004
[5] Ju J, Saito H, Kurumaji T, Hirschberger M, Kikkawa A, Taguchi Y, Arima T H, Tokura Y and Nakajima T 2023 Phys. Rev. B 107 024405
[6] Musgrave M M, Baeßler S, Balascuta S, Barrón-Palos L, Blyth D, Bowman J D, Chupp T E, Cianciolo V, Crawford C, Craycraft K, Fomin N, Fry J, Gericke M, Gillis R C, Grammer K, Greene G L, Hamblen J, Hayes C, Huffman P, Jiang C, Kucuker S, McCrea M, Mueller P E, Penttilä S I, Snow W M, Tang E, Tang Z, Tong X and Wilburn W S 2018 Nucl. Instrum. Methods Phys. Res. Sect. A 895 19-28
[7] Coulter K P, Chupp T E, McDonald A B, Bowman C D, Bowman J D, Szymanski J J, Yuan V, Cates G D, Benton D R and Earle E D 1990 Nucl. Instrum. Methods Phys. Res. Sect. A 288 463-466
[8] Tong X, Jiang C Y, Lauter V, Ambaye H, Brown D, Crow L, Gentile T R, Goyette R, Lee W T, Parizzi A and Robertson J L 2012 Rev. Sci. Instrum. 83 075101
[9] Andersen K H, Jullien D, Petoukhov A K, Mouveau P, Bordenave F, Thomas F and Babcock E 2009 Physica B 404 2652-2654
[10] Wang Y T, Wu L Y, Zhang K Y, Peng M, Chen S Y and Yan H Y 2024 Sci. Chin. Phys. Mech. Astron. 67 273011
[11] Yan S, Zhang M F, Guo W C, Wang W Z, Gong J, Liang T J, Liu B Q, Peng M, Peng S M, Sun G A, Tu X Q, Yan H Y, Zhang J H and Zheng H 2019 Sci. Chin. Phys. Mech. Astron. 10 102021
[12] Jiang C Y, McDonald L, Cao H, Balafas M, Crow L and Kroll E 2023 J. Phys.: Conf. Ser. 2481 012010
[13] Kira H, Sakaguchi Y, Oku T, Suzuki J, Nakamura M, Arai M, Endoh Y, Chang L J, Kakurai K, and Arimoto Y, Ino T, Shimizu H M, Kamiyama T, Ohoyama K, Hiraka H, Tsutsumi K and Yamada K 2011 J. Phys.: Conf. Ser. 294 012014
[14] Huang C Y, Zhang J P, Ye F, Qin Z C, Amir S M, Buck Z N, Salman A, Kreuzpaintner W, Qi X, Wang T H and Tong X 2021 Chin. Phys. Lett. 38 092801
[15] Zhang J P, Huang C Y, Qin Z C, Ye F, Amir S M, Salman A, Dong Y C, Tian L, Buck Z N, Kreuzpaintner W, Musgrave M, Qi X, Wang T H and Tong X 2022 Sci. Chin. Phys. Mech. Astron. 65 241011
[16] Gentile T R, Nacher P J, Saam B and Walker T G 2017 Rev. Mod. Phys. 89 045004
[17] COMSOL Multiphysics v6.0. COMSOL AB (Stockholm, Sweden, 2023)
[18] Cates G D, Schaefer S R and Happer W 1988 Phys. Rev. A 37 2877
[19] McIver J W, Erwin R, Chen W C and Gentile T R 2009 Rev. Sci. Instrum. 80 063905
[20] Guo S H 2008 Electrodynamics (3rd ed.) (Beijing: Higher Education Press) pp 80-81 (in Chinese)
[21] Chann B, Babcock E, Anderson L W and Walker T G 2002 Phys. Rev. A 66 032703
[22] Wang B, Zhang J P, Lu Y P, Huang C Y, Wang T H, Qin Z C, Dong Y C, Zheng Y J, Li J, Zhang W Q, Ye F, Qi X, Liu Y T and Tong X 2023 J. Appl. Phys. 133 173105
[23] F. ANSYS Inc., Ansys Fluent Theory Guide (Ansys Inc., USA, 2011)
[24] Qin Z C, Huang C Y, Buck Z N, Kreuzpaintner W, Amir S M, Salman A, Ye F, Zhang J P, Jiang C Y, Wang T H and Tong X 2021 Chin. Phys. Lett. 38 052801
[25] McKetterick T J, Boag S, Stewart J R, Frost C D, Skoda M W A, Parnell S R and Babcock E 2010 Physica B 406 2436-2438
[26] Ino T 2018 Proceedings of the International Conference on Neutron Optics p 011016
[27] Boag S, Babcock E, Andersen K H, Becker M, Charlton T R, Chen W C, Dalgliesh R M, Elmore S D, Frost C D, Gentile T R, Lopez Anton R, Parnell S R, Petoukhov A K, Skoda M W A and Soldner T 2009 Physica B 404 2659-2662
[28] Salhi Z, Babcock E, Bingöl K, Bussmann K, Kammerling H, Ossovyi V, Heynen A, Deng H, Hutanu V, Masalovich S, Voigt J and Ioffe A 2019 J. Phys.: Conf. Ser. 1316 012009
[29] Jiang C Y, Tong X, Brown D R, Chi S, Christianson A D, Kadron B J, Robertson J L and Winn B L 2014 Rev. Sci. Instrum. 85 075112
[30] Kira H, Sakaguchi Y, Oku T, Suzuki J, Nakamura M, Arai M, Endoh Y, Chang L J, Kakurai K, Arimoto Y, Ino T, Shimizu H M, Kamiyama T, Ohoyama K, Hiraka H, Tsutsumi K and Yamada K 2011 J. Phys.: Conf. Ser. 294 012014
[31] Jiang C Y 2023 AAPPS Bulletin 33 21
[32] Zhu T, Zhan X Z, Xiao S W, Sun Y, Wu Y Y, Zhou A Y and Han Q F 2018 Neutron News 29 11-13
[33] Zhang M F, Yang Z, Zhang J P, Huang C Y, Wang T H, Chen Y H, Fan R R, Snow W M and Tong X 2024 Nucl. Instrum. Methods Phys. Res. Sect. A 170184